

Journal of Materials Chemistry A

Accepted Manuscript



This is an *Accepted Manuscript*, which has been through the Royal Society of Chemistry peer review process and has been accepted for publication.

Accepted Manuscripts are published online shortly after acceptance, before technical editing, formatting and proof reading. Using this free service, authors can make their results available to the community, in citable form, before we publish the edited article. We will replace this *Accepted Manuscript* with the edited and formatted *Advance Article* as soon as it is available.

You can find more information about *Accepted Manuscripts* in the [Information for Authors](#).

Please note that technical editing may introduce minor changes to the text and/or graphics, which may alter content. The journal's standard [Terms & Conditions](#) and the [Ethical guidelines](#) still apply. In no event shall the Royal Society of Chemistry be held responsible for any errors or omissions in this *Accepted Manuscript* or any consequences arising from the use of any information it contains.



Journal Name

ARTICLE

2D amorphous iron phosphate nanosheets with high rate capability and ultra-long cycle life for sodium ion batteries

Tongchao Liu^a, Yandong Duan^a, Guangxing Zhang^a, Maofan Li^a, Yancong Feng^a, Jiangtao Hu^a, Jiaxin Zheng^a, Jitao Chen^{ab} and Feng Pan^{*a}

Received 00th January 20xx,
Accepted 00th January 20xx

DOI: 10.1039/x0xx00000x

www.rsc.org/

In our previous work, we reported formation and its mechanism of mono/bi-layer phosphate-based material and high performance as a cathode material for Li-ion batteries.¹ In this work, we report the 2D amorphous nanosheets were used as cathode materials to achieve outstanding performance for sodium ion batteries (SIBs) e.g. high initial discharge capacity of 168.9 mAh g⁻¹ at 0.1 C, ultra-long life (92.3% capacity retention over 1000 cycles), and high rate capability (77 mAh g⁻¹ at 10 C) for Na-ion storage, which electrochemical performance is also much superior to the reported amorphous FePO₄ or olivine NaFePO₄ with advantages of short paths and larger implantation surface areas for fast Na⁺-ion diffusion and large specific surfaces with more interface capacitance. Interestingly, NaFePO₄ nano-crystals with about 10 nm sizes are self-nucleated from amorphous 2D nanosheets in the charge/discharge process, which was verified by transmission electron microscopy (TEM) and in-situ electrochemical impedance spectroscopy (EIS).

Introduction

Lithium (Li)-ion batteries (LIBs) are the modern high-performance energy storage devices for portable electronics and increasingly for electrical vehicles due to their high energy and power densities.² However, with the increasingly serious energy crisis, the extensive application of LIBs faces important challenges related to both Li availability and cost.³ Using sodium-ion batteries (SIBs) as an alternative attracted great interest, because Na is more abundant than Li and is easy to recover.⁴ In addition, the intercalation chemistry of Na and Li is similar, thus the known LIB knowledge can be exploited in SIB.⁵ Nevertheless, many challenges need to overcome before SIBs can become commercially competitive with LIBs. For instance, compared with lithium, sodium weighs more and has a higher ionization potential and a larger ionic radius, which led to a lower theoretical capacity and poor rate capability.

Since the performance of SIBs (e.g., specific capacity and operation voltage) is largely dependent on the electrochemical properties of the electrode materials, it is of great importance to develop suitable electrode materials for SIBs.⁶⁻⁸ Among them,

phosphate-based materials have been identified as potential electroactive materials for SIBs,⁹ such as NaFePO₄ (olivine),¹⁰⁻¹³ NaVPO₄F,¹⁴⁻¹⁶ Na₃V₂(PO₄)₂F₃,¹⁷⁻¹⁹ Na_{1.5}VOPO₄F_{0.5},^{20,21} Na₂FePO₄F,²² Na₃V₂(PO₄)₃,²³⁻²⁶ Na₃Al₂(PO₄)₂F₂,^{27,28} Na₂NiPO₄F,²⁹ Na₂(Fe_{1-x}Co_x)PO₄F³⁰ and Na₂(Fe_{1-x}Mg_x)PO₄F³¹, etc. However, crystalline phosphates have so far performed poor electrochemical performance for SIBs, because the undersized channel of lattice limits the diffusion of Na ion. Thus, compared with LIBs, the crystalline phosphate-based sodium cathode materials show poor rate capability and cycling stability,^{32,33} which limits commercial development of SIBs.

In previous work¹, we reported the formation of a special amorphous mono/bi-layer phosphate-based material and performance as a cathode material for LIBs, with some natural advantages such as: shorter paths and larger implantation surface areas for fast Li-ion diffusion and large specific surfaces with more interface capacitance. When applied in LIBs, it shows excellent performance with high capacity and rate capability. In view of above natural advantages, such 2D nanosheets should have excellent performance when applied in sodium ion batteries. Herein, we used previous methods to synthesize mono/bi-layer iron phosphate 2D nanosheets to use as a novel cathode for SIBs, which show excellent performance: high initial discharge capacity of 168.9 mAh g⁻¹ at 0.1 C, ultra-long life (92.3% capacity retention over 1000 cycles), and high rate capability (77 mAh g⁻¹ at 10 C) for Na-ion storage. Interestingly, NaFePO₄ nano-crystals are self-

a. School of Advanced Materials, Peking University, Peking University Shenzhen Graduate School, Shenzhen 518055, China. Tel: 86-755-26033200; E-mail: panfeng@pkusz.edu.cn

b. Beijing National Laboratory for Molecular Sciences, College of Chemistry and Molecular Engineering, Peking University, Beijing 100871, China
Electronic Supplementary Information (ESI) available: [experimental procedures, figures and tables.]. See DOI: 10.1039/x0xx00000x

nucleated by electrochemical forces driven from the oxidation of amorphous 2D nanosheets during charge/discharge process.

Experimental

Materials

These atomically thin amorphous 2D-sheets are controllably prepared through a simple chemically induced precipitation method and post-processing, which is the same as our previous work.¹ The two main fabrication steps are the preparation of precursor and post-processing by water and ethanol. For the preparation of precursor, $\text{FeSO}_4 \cdot 7\text{H}_2\text{O}$, H_3PO_4 , and $\text{LiOH} \cdot \text{H}_2\text{O}$ were used as starting materials. Firstly, 1.05 g $\text{FeSO}_4 \cdot 7\text{H}_2\text{O}$ was dissolved in 33.30 g of ethylene glycol with nitrogen protection. Secondly, 0.55 g H_3PO_4 was mixed in 8.80 g of ethylene glycol, then the solution was slowly introduced to the FeSO_4 solution under stirring. Third, 0.43 g LiOH was added into 41.6 g of ethylene glycol, dissolved under ultrasonic treatment, then the solution was added into the prior mixed solution, resulting in a dark green precursor. For the post-processing, the precursor was washed twice with water and once with ethanol. Finally, the product was dried in vacuum drying oven at 80 °C.

Material characterization

X-ray powder diffraction patterns were collected from a Bruker D8 Advance diffractometer with $\text{Cu K}\alpha$ ($\lambda = 0.15418$ nm) at the

2θ range of 10–80° with a step of 0.02° and a testing time of 1 s. The morphologies were observed by using SEM (ZEISS Supra 55) and TEM (FEI Tecnai G2 F20 S-Twin). The energy-dispersive spectroscopy (EDS) was observed by using an Oxford-Max20 detector attached to the SEM. The thickness of nanosheets was measured by using AFM (Bruker MultiMode 8).

Electrochemical measurements

Electrochemical characterization was measured by 2032 coin cells. For the cathode, FePO_4 @C and PTFE (Polytetrafluoroethylene) binder were mixing in the isopropanol, in which the weight ratio was 80:20. With grinding in the agate mortar, FePO_4 @C and PTFE binder were mixed evenly, resulting into the cathode plate, and then dried in vacuum at 110 °C for 12 h. Sodium metal anodes were prepared by cutting and planishing sodium pieces. The 2032 coin cells were assembled by the above cathode plates, sodium metal anodes and electrolytes. All the cells were assembled in a glove box tested at room temperature. The electrochemical characteristics of cells were conducted on a NEWARE battery cycler in the voltage range of 1.4–3.8 V (vs. Na^+/Na). The cyclic voltammetry (CV) results were obtained by a CHI 604E. (Chenhua Instruments Co., China). The electrochemical impedance spectra were collected from 10^4 to 0.1 Hz and the amplitude was 10 mV.

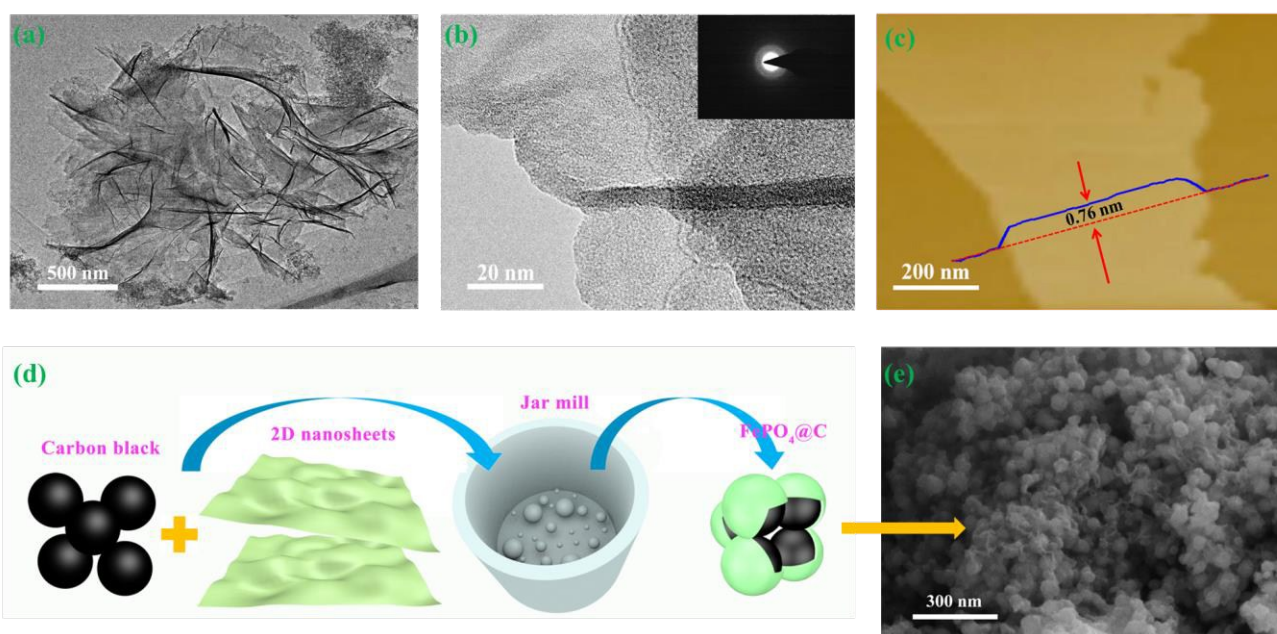


Fig. 1 (a) TEM image of 2D nanosheets (b) High-resolution TEM (HR-TEM) images of the 2D nanosheets. The inset is selected area electron diffraction image of the 2D nanosheets. (c) AFM image of a typical nanosheet with a thickness of 0.74 nm, corresponding to one atomic layer. (d) The schematics of formed hybrid cathode materials ($\text{Fe}(\text{II})_3(\text{PO}_4)_2 \cdot \text{Fe}(\text{III})_3(\text{PO}_4)_2(\text{OH})_3 \cdot n\text{H}_2\text{O}/\text{C}$ ("FP@C")) by mixing the 2D nanosheets with carbon black by ball milling. (e) The SEM images for the mixture of nanosheets and carbon black.

Results and discussion

Fig. 1 shows the morphology of as-prepared amorphous 2D nanosheets for this work characterized by TEM and AFM, and the schematics of formed hybrid cathode materials ($\text{Fe(II)}_3(\text{PO}_4)_2 \cdot \text{Fe(III)}_3(\text{PO}_4)_2(\text{OH})_3 \cdot n\text{H}_2\text{O}/\text{C}$ ("FP@C")) by mixing the 2D nanosheets with carbon black by ball milling. The SEM and TEM images show large scale nanosheets prepared for this work with an average size of more than $1 \mu\text{m}$ (Fig. S1, S2, S3 and Fig. 1a). High-resolution TEM images clearly illustrate no crystal lattice (Fig. 1b), and the Selected Area Electron Diffraction (SAED) images also show no signals of crystalline diffraction spots, indicating the amorphous structure for the prepared 2D nanosheets, which was further indicated by X-Ray Diffraction (XRD), as shown in Fig. S5. The thicknesses of the thin films measured by AFM are 0.76 nm and 1.55 nm, as shown in Fig. 1c and S4. In order to make full use of 2D nanosheets natural advantages, we created the 2D nanosheets coating carbon black special structure, where the 2D nanosheets were triturated and evenly coated on the surface of carbon black by ball milling (Fig. 1d). Therefore, 2D nanosheets have close contact with carbon black, and carbon black forms excellent conductive network. After ball milling process, the 2D nanosheets still kept amorphous structure, indicated by XRD (Fig. S5). The SEM images and EDS mapping show that the 2D nanosheets and carbon black had been fully mixed together as "FP@C" (Fig. 1e and S6).

To demonstrate the advantages of these 2D nanosheets, we evaluate their performance as cathode materials for SIBs, in which the sodium metal was used as the counter electrode and a mixture of EC and DMC with 1M NaClO_4 dissolved was used as electrolyte.³⁴ Fig. 2a shows the charge/discharge curves of the 2D nanosheets hybrid cathode within a cut-off voltage window of 1.4–3.8 V versus Na^+/Na at a current rate of 0.1 C ($1 \text{ C} = 170 \text{ mA g}^{-1}$). The first discharge capacity is very high, about 168.9 mAh g^{-1} . Note that because of the absence of sodium ion, Fe(II) in FP@C is oxidized to Fe(III) in the first charge with a capacity of about 9.5 mAh g^{-1} . After the second charge/discharge cycle, the electrode delivers normal charge and discharge curves. These 2D nanosheets also show excellent rate capability at charge/discharge current rates ranging from 0.1–10 C, as shown in Fig. 2b. The average capacities are 168, 145, 132, 116, 96, and 77 mAh g^{-1} at charge/discharge current rates of 0.1, 0.5, 1, 2, 5 and 10 C, respectively. After high-rate charge/discharge cycling, a specific capacity of 170.1 mAh g^{-1} is restored when the current density is back to 0.1 C. All these results indicate that 2D nanosheets exhibit an excellent rate capability and electrochemical reversibility for sodium ion storage. To the best of our knowledge, this excellent rate capability is reported for the first time in types of olivine NaFePO_4 and amorphous FePO_4 . The cycling performance of the 2D nanosheets was measured at a current density of 1 C, as shown in Fig. 2c. After 1000 cycles, the capacity declines slightly from 127.8 to 117.9 mAh g^{-1} , by a

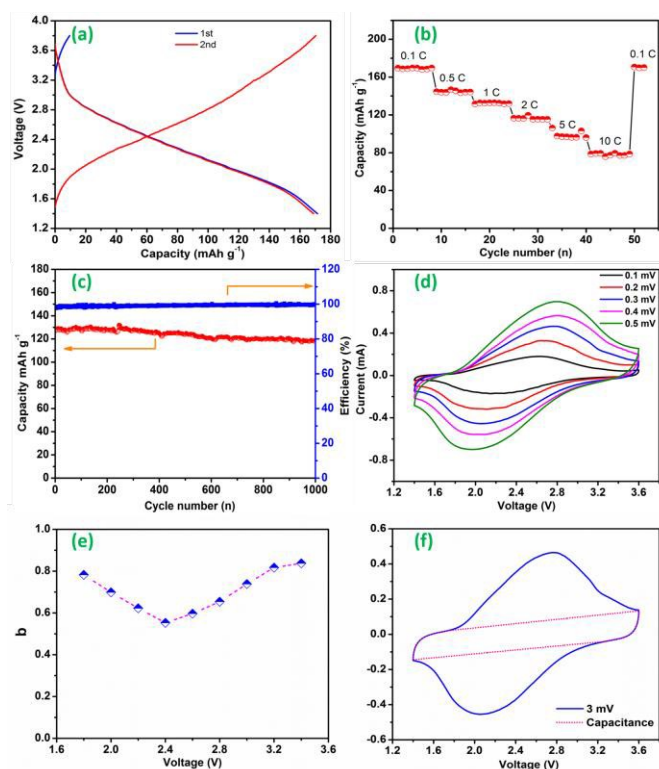


Fig. 2 (a) Galvanostatic discharging/charging profiles obtained at 0.1 C. (b) Capacity versus cycle number at 0.1 C, 0.5 C, 1 C, 2 C, 5 C, 10 C and return to 0.1 C. (c) Cycling performance of the sodium ion battery of 2D nanosheets. The capacity retention at 1 C is about 92.3%, declining from 127.8 mAh g^{-1} at the first cycle to 117.9 mAh g^{-1} at the 1000th cycle. (d) CV curves conducted at scan rates of 0.1 mV s^{-1} to 0.5 mV s^{-1} . (e) The b-values of the different voltages. (f) CV curves and the capacitance contribution.

factor of 7.7%, which is superior to those reported types of NaFePO_4 materials. The cyclic voltammogram (CV) curve shows a pair of current peaks positioned at 2.6 and 2.2 V (Fig. 2d), corresponding to the deintercalation/intercalation of sodium ion, respectively. The broad deintercalation peaks imply a continuous single-phase deintercalation reaction, which is quite different from that of the olivine NaFePO_4 characterized by a biphasic transition during the sodium ion de-intercalation/intercalation.

Table 1 shows a comparison of our work with the reported works on SIBs based on amorphous FePO_4 or olivine NaFePO_4 with high performance. Hu³⁵ reported that porous amorphous FePO_4 nanoparticles mixed with single-wall carbon nanotubes showed cell performance for Na-ions storage. The electrochemical performance shows the discharge capacity is 120 mAh g^{-1} at 0.1 C rate (10 mA g^{-1}), and the capacity still remain 50 mAh g^{-1} after 300 cycles at 1 C rate (100 mA g^{-1}). Cao³⁶ reported amorphous FePO_4 nanospheres showed high-performance for sodium ion batteries with a high initial discharging capacity of 151 mAh g^{-1} at 20 mA g^{-1} , good cycle stability (94% capacity retention ratio over 160 cycles), as well as high rate capability (44 mAh g^{-1} at 1000 mA g^{-1}). Xu³⁷ reported amorphous FePO_4 nano-

Table 1 The comparison of our work with the reported works on SIBs based on amorphous FePO₄ or olivine NaFePO₄.

Compound	Capacity (mAh g ⁻¹)	Rate Capacity (mAh g ⁻¹)	Cycling performance
Our paper	169 (0.1 C)	77 (10 C)	92.3% (1000cycle 1C)
Amorphous-FePO ₄ ³⁵	120 (0.1 C)	50 (1 C)	98% (40cycle 0.5C)
Amorphous-FePO ₄ ³⁶	151 (0.1 C)	44 (10 C)	94% (160cycle 0.1C)
Amorphous-FePO ₄ ³⁷	142 (0.1 C)	64 (1 C)	92% (120cycle 0.1C)
Amorphous-FePO ₄ ³⁸	155 (0.1 C)	75 (1 C)	--
Maricite-NaFePO ₄ ¹²	142 (0.05 C)	66 (2 C)	95% (200cycle 0.1C)
Olivine-NaFePO ₄ ³³	111 (0.1 C)	46 (2 C)	90% (240cycle 0.1C)
Olivine-NaFePO ₄ ³⁹	120 (0.05 C)	25 (2 C)	90% (100cycle 0.1C)
Olivine-NaFePO ₄ ¹¹	125 (0.05 C)	85 (0.5 C)	90% (50cycle 0.1C)

particles showed an initial specific-discharge capacity of 142 mAh g⁻¹, reversible capacity of 130.8 mAh g⁻¹ after 120 cycles, and high rate capability of 63.5 mA h g⁻¹ at 1 C. Liu³⁸ reported FePO₄@MCNT nanowire showed excellent cell performance with a discharge specific capacity of 155.2 mAh g⁻¹ in the initial cycle and 157.2 mAh g⁻¹ after 70 cycles at 0.1 C. From Table 1, we can see that our 2D nanosheets shows the best electrochemical performance in all reported.

The reasons for the 2D nanosheets showed the remarkable electrochemical performance with high capacity, high rate capacity, and long life can be attributed as below. Compared with amorphous FePO₄ and olivine NaFePO₄, the 2D nanosheets create shorter paths and larger implantation surface areas for fast Li/Na-ion diffusion. The energy barrier of Na ion insertion of 2D-Na is much lower than that in bulks of olivine NaFePO₄. Because of larger ionic radius, Na ion is difficult to insert into undersized channel of bulks of olivine NaFePO₄. For 2D nanosheets, the diffusion of sodium ion is not limited in mono/bi-layer materials. Another reason is that large surfaces of the 2D nanosheets would contribute large interface capacitance to the total capacity. Similar to 2D nanosheets in lithium ion batteries, to investigate the effect of the capacitance-type behavior of 2D nanosheets on their electrochemical performance, we measured a series of CV curves at scan rates of 0.1-0.5 mV s⁻¹. The shapes of these CV curves (Fig. 2d) show no distortion with the speeding up of the scanning rate, meaning that the 2D nanosheets exhibit an excellent rate capability. Assuming that the current and the scan rate follow a power-law relationship,⁴⁰ $I_p = av^b$, where a and b are adjustable values. b value of 0.5 indicates that the current is controlled by semi-infinite linear diffusion, while b value of 1 indicates that the current is surface-controlled like capacitance.⁴¹ We get the b-values at 1.8-3.6 V are between 0.503 and 0.838, indicating a concurrence of both sodium ion semi-infinite linear diffusion and surface-controlled pseudocapacitance. (Fig. 2e). We further investigated the capacitance contribution in the sodium ion battery capacity, as

shown in Fig. 2f. According to CV curves, electric quantity of the whole cycle and capacitance part were calculated separately by a numerical integration. The results show the capacitive contribution in the sodium ion battery is almost unchanged at any scan rate, and interface capacitance accounted for 31.7%-33.8% of the total capacity, as shown in Fig. S7.

We further compared the electrochemical performance of 2D nanosheets SIBs (2D-Na) with that of 2D nanosheets LIBs (2D-Li). As shown in Fig. 3a, the average voltage of the discharge curve of 2D-Na is lower than that of 2D-Li by 0.31 V, which is smaller than the voltage reduction of 0.53 V from olivine LiFePO₄ to NaFePO₄.⁴² In addition, compared with bulk crystalline materials, the variation of the rate capability between 2D-Li and 2D-Na is much smaller (Fig. 3b). For example, the capacity of bulk olivine NaFePO₄ is decreased from 120 mAh g⁻¹ @ 0.1 C to 40 mAh g⁻¹ @ 2 C, 2.5 times larger than the capacity decrease for olivine LiFePO₄ (168 mAh g⁻¹ @ 0.1 C vs. 120 mAh g⁻¹ @ 2 C). In contrast, the capacity of 2D-Na is decreased from 169 mAh g⁻¹ @ 0.1 C to 77 mAh g⁻¹ @ 10 C, 1.5 times larger than the capacity decrease for 2D-Li (185 mAh g⁻¹ @ 0.1 C and 127 mAh g⁻¹ @ 10 C for 2D-Li). The much better rate capability performance of 2D-Na is due to the absence of the undersized channel for diffusion. We further compared the resistance of 2D-Li and 2D-Na (Fig. 3c), and the data are analyzed according to the following equation:⁴³

$$D_{Li^+} = R^2 T^2 / 2A^2 n^4 F^4 C^2 \kappa^2$$

where R is the gas constant, T is the absolute temperature, A is the surface area of the electrode, n is the number of electrons per molecule, F is the Faraday constant, C is the concentration of Li-ion, and κ is the Warburg factor to be determined from the slope of the low frequency part of resistance. It can be seen that 2D-Li and 2D-Na have the similar κ , so the diffusion

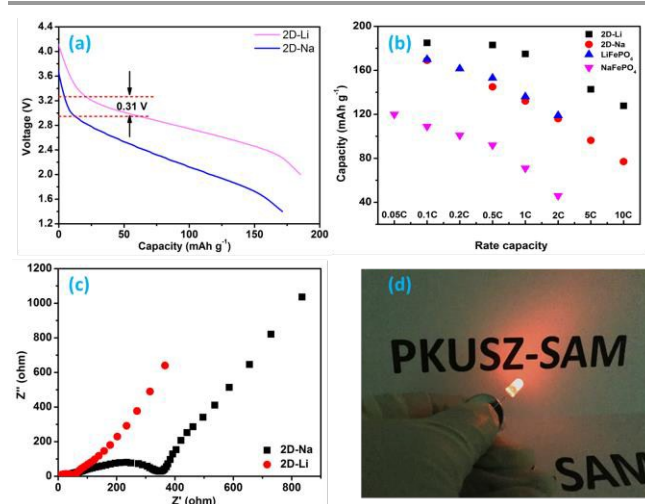


Fig. 3 (a) Discharge curve of 2D-Na and 2D-Li. (b) Rate capability of 2D-Li, 2D-Na, LiFePO₄ and NaFePO₄. (c) Electrochemical impedance spectroscopy (EIS) of 2D-Li and 2D-Na. (d) The image of LED lit by 2D nanosheets sodium ion battery.

coefficients of those are similar, which further indicates 2D nanosheets with shorter diffusion paths for cation storage.

Electrochemical impedance spectroscopy (EIS) is used to study the electrode reaction kinetics of 2D-Na. We tested the EIS of the coin cell after 1, 10, 20, 40, and 100 cycles at 1 C as shown in Fig. 4a and Fig. S8, in which the visible semicircles in the high and middle frequency ranges reflect the solid-electrolyte interface (SEI) resistance (R_{sei}) and charge transfer resistance (R_{ct}), respectively. Similar to the ref 1, the third semicircle appears in the low frequency ranges with charge/discharge cycles, which indicates additional diffusion behavior appears in semi-infinite linear diffusion. We speculate that the additional diffusion behavior is associated with the formation of NaFePO_4 nano-crystalline particles as the new “second-phase” (see Fig. 4c-d). The “transmission line model” is proposed to explain the special EIS features. Due to the presence of amorphous and crystal phase in the 2D nanosheets, the Na^+ can diffuse into/from the amorphous phase and NaFePO_4 nano-crystalline particles during discharge/charge process, which leads to two kinds of diffusion behavior and the second semicircle.

To further validate the second phase generated after cycling, we dismantled the coin cell after 1000 cycles at 1 C and cleaned the electrode materials for EDS, XRD and TEM analyses. The EDS mapping (Fig. S9) shows Na ion insertion into the 2D nanosheets. Fig. 4b shows the XRD patterns of the electrode materials with strong reflection peaks at 28.2 and 41.4, which correspond to the phase structure of (020) and (212) planes of crystalline NaFePO_4 , respectively. TEM (Fig. S10 and Fig. 4c) images show that the morphology of 2D nanosheets remains

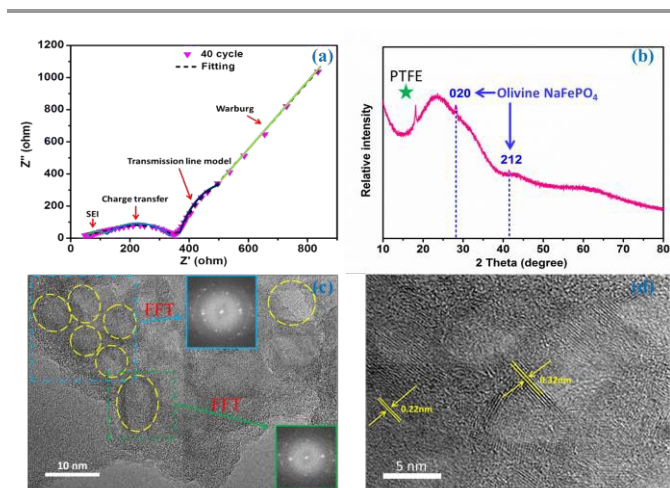


Fig. 4 (a) Electrochemical impedance spectroscopy (EIS) and the fitting curve for 40 charge/discharge cycles. (b) XRD pattern for crystallization of nanosheets after 1000 cycles. (c) TEM image for crystallization of 2D nanosheets. The inset is the FFT figure of 2D nanosheets. (d) HR-TEM image for crystallization of 2D nanosheets.

unchanged and many nano-crystal particles with 10-15 nm sizes are inside of the 2D nanosheets. Furthermore, the high magnification TEM images (Fig. 5d and Fig. S11) revealed the obvious lattice channels in the nano-particles with two kinds of interplanar distance of about 0.22 nm and 0.32 nm. This finding is consistent with the d_{212} value (0.22 nm) and d_{020} value (0.32 nm), calculated from the XRD pattern of olivine NaFePO_4 crystals. Thus, both TEM and XRD results strongly prove that olivine NaFePO_4 nano-crystals can be nucleated and grown from atomically thin amorphous 2D nanosheets in the electrochemical charge/discharge cycles. The nucleation and limited sizes (about 10-15 nm) of NaFePO_4 nano-crystals from amorphous are interesting. Its mechanism can be proposed that NaFePO_4 -like short-ordering structures in the amorphous 2D nanosheets can become nucleated-centers, but it is hard to grow a nucleus in big size because of the high mobility resistance of the iron phosphate group in the solid amorphous phase. The ratio of NaFePO_4 nano-crystalline part and amorphous part left without crystalline is difficult to be defined.

Conclusions

We use the synthesized mono/bi-layer amorphous iron phosphate nanosheets milled with carbon black to generate hybrid cathode materials for SIBs, which show a high reversible capacity of 168.9 mAh g^{-1} @ 0.1 C, high rate capability of 77 mAh g^{-1} @ 10 C, and an excellent cycling stability with 92.3% capacity retention after 1000 cycles. This electrochemical performance is also superior to the reported high performance of SIBs based on amorphous FePO_4 or olivine NaFePO_4 . The high performance can be attributed to the shorter paths and larger implantation surface areas for fast Na-ion diffusion and more interface capacitance in such mono/bi-layer amorphous iron phosphate nanosheets. Interestingly, self-nucleated NaFePO_4 nano-crystals with sizes of about 10-15 nm as the new phase can be in-situ observed by EIS during the electrochemical charge/discharge cycles. This work reveals that the atomically thin 2D nanosheets can become novel electrode materials with hybrid behavior of battery and supercapacitor for high-performance sodium ion batteries.

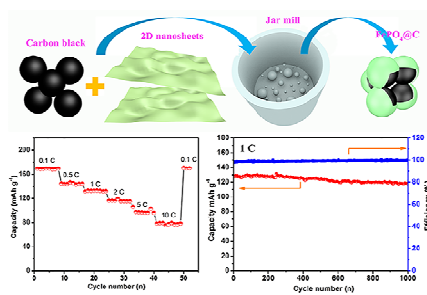
Acknowledgements

The research was financially supported by Guangdong Innovation Team Project (No. 2013N080) and Shenzhen Science and Technology Research Grant (peacock plan KYPT20141016105435850).

References

1. T. Liu, Y. Feng, Y. Duan, S. Cui, L. Lin, J. Hu, H. Guo, Z. Zhuo, J. Zheng and Y. Lin, *Nano Energy*, 2015, **18**, 187-195.
2. Tarascon, J. M. Amp and M. Armand, *Nature*, 2001, 359-367.
3. H. L. Pan, Y. S. Hu and L. Q. Chen, *Energy Environ Sci*, 2013, **6**, 2338-2360.
4. V. Palomares, P. Serras, I. Villaluenga, K. B. Hueso, J. Carretero-González and T. Rojo, *Energy Environ Sci*, 2012, **5**, 5884-5901.
5. M. S. Islam and C. A. J. Fisher, *Chemical Society Reviews*, 2014, **45**, 185-204.
6. Y. Naoaki, K. Kei, D. Mouad and K. Shinichi, *Chemical Reviews*, 2014, **114**, 11636-11682.
7. C. M. L. Croguennec, *chemical reviews*, 2013, **113**, 6552-6591.
8. K. Haegyeom, H. Jihyun, P. Kyu-Young, K. Hyungsub, K. Sung-Wook and K. Kisuk, *Chemical Reviews*, 2014, **114**, 11788-11827.
9. J. Lu, S. C. Chung, S. I. Nishimura and A. Yamada, *Chemistry of Materials*, 2013, **25**, 3480-3487.
10. P. Moreau, D. Guyomard, J. Gaubicher and F. Boucher, *Chemistry of Materials*, 2010, **22**, 4126-4128.
11. S. M. Oh, S. T. Myung, J. Hassoun, B. Scrosati and Y. K. Sun, *Electrochemistry Communications*, 2012, **22**, 149-152.
12. J. Kim, D. H. Seo, H. Kim, I. Park, J. K. Yoo, S. K. Jung, Y. U. Park, W. A. G. Iii and K. Kang, *Energy & Environmental Science*, 2015, **8**, 540-545.
13. M. Casas-Cabanas, V. V. Roddatis, D. Saurel, P. Kubiak, J. Carretero-González, V. Palomares, P. Serras and T. Rojo, *J.mater.chem*, 2012, **22**, 17421-17423.
14. J. Zhao, J. He, X. Ding, J. Zhou, Y. O. Ma, S. Wu and R. Huang, *Journal of Power Sources*, 2010, **195**, 6854-6859.
15. Y. Lu, S. Zhang, Y. Li, L. Xue, G. Xu and X. Zhang, *Journal of Power Sources*, 2014, **247**, 770-777.
16. M. W. Xu, C. Cheng, Q. Q. Sun, S. J. Bao, Y. B. Niu, H. He, Y. Li and J. Song, *Rsc Advances*, 2015, **5**, 40065-40069.
17. C. Zhu, K. Song, P. A. van Aken, J. Maier and Y. Yu, *Nano Letters*, 2014, **14**, 2175-2180.
18. M. Bianchini, N. Brisset, F. Fauth, F. Weill, E. Elkaim, E. Suard, C. Masquelier and L. Croguennec, *Chemistry of Materials*, 2014, **26**, 4238-4247.
19. Z. Liu, Y.-Y. Hu, M. T. Dunstan, H. Huo, X. Hao, H. Zou, G. Zhong, Y. Yang and C. P. Grey, *Chemistry of Materials*, 2014, **26**, 2513-2521.
20. A. A. Tsirlin, R. Nath, A. M. Abakumov, Y. Furukawa, D. C. Johnston, M. Hemmida, H. A. K. V. Nidda, A. Loidl, C. Geibel and H. Rosner, *Physical Review B*, 2011, **84**, 44-44.
21. F. Sauvage, E. Quarez, J. M. Tarascon and E. Baudrin, *Cheminform*, 2007, **38**, no-no.
22. M. Ramzan, S. Lebègue, P. Larsson and R. Ahuja, *Journal of Applied Physics*, 2009, **106**, 043510-043516.
23. J. Gopalakrishnan and K. K. Rangan, *Chemistry of Materials*, 1992, **4**, 745-747.
24. K. Saravanan, C. W. Mason, A. Rudola, K. H. Wong and P. Balaya, *Advanced Energy Materials*, 2013, **3**, 444-450.
25. Z. Jian, W. Han, X. Lu, H. Yang, Y. S. Hu, J. Zhou, Z. Zhou, J. Li, W. Chen and D. Chen, *Advanced Energy Materials*, 2013, **3**, 138-138.
26. S. Li, Y. Dong, L. Xu, X. Xu, L. He and L. Mai, *Advanced Materials*, 2014, **26**, 3545-3553.
27. J.-M. Le Meins, M.-P. Crosnier-Lopez, A. Hemon-Ribaud and G. Courbion, *Journal of solid state chemistry*, 1999, **148**, 260-277.
28. J.-M. Le Meins, O. Bohnke and G. Courbion, *Solid State Ionics*, 1998, **111**, 67-75.
29. B. L. Ellis, W. M. Makahnouk, W. Rowan-Weetaluktuk, D. Ryan and L. F. Nazar, *Chemistry of Materials*, 2009, **22**, 1059-1070.
30. B. Prabeer, C. Jean-No?L, R. Nadir, D. Charles, A. Mohamed, D. Loic, A. Michel and T. Jean-Marie, *Cheminform*, 2010, **49**, 7401-7413.
31. M. Avdeev, C. D. Ling, T. T. Tan, S. Li, G. Oyama, A. Yamada and P. Barpanda, *Inorganic chemistry*, 2013, **53**, 682-684.
32. A. Sun, F. R. Beck, D. Haynes, J. A. Poston, S. Narayanan, P. N. Kumta and A. Manivannan, *Materials Science and Engineering: B*, 2012, **177**, 1729-1733.
33. Y. Fang, Q. Liu, L. Xiao, X. Ai, H. Yang and Y. Cao, *Acs Applied Materials & Interfaces*, 2015, **7**.
34. A. Ponrouch, E. Marchante, M. Courty, J. M. Tarascon and M. R. Palacín, *Energy & Environmental Science*, 2012, **5**, 8572-8583.
35. Y. Liu, Y. Xu, X. Han, C. Pellegrinelli, Y. Zhu, H. Zhu, J. Wan, A. C. Chung, O. Vaaland and C. Wang, *Nano Letters*, 2012, **12**, 5664-5668.
36. Y. Fang, L. Xiao, J. Qian, X. Ai, H. Yang and Y. Cao, *Nano Letters*, 2014, **14**, 3539-3543.
37. Y. Liu, Y. Zhou, J. Zhang, S. Zhang and S. Xu, *Physical Chemistry Chemical Physics*, 2015, **17**, 22144-22151.
38. S. Xu, S. Zhang, J. Zhang, T. Tan and Y. Liu, *J.mater.chem.a*, 2014, **2**, 7221-7228.
39. Z. Yujie, X. Yunhua, L. Yihang, L. Chao and W. Chunsheng, *Nanoscale*, 2013, **5**, 780-787.
40. J. Come, P. L. Taberna, S. Hamelet, C. Masquelier and P. Simon, *Journal of the Electrochemical Society*, 2011, **158**, A1090-A1093.
41. A. Veronica, C. Jérémy, M. A. Lowe, K. Jong Woung, T. Pierre-Louis, S. H. Tolbert, H. D. Abruna, S. Patrice and D. Bruce, *Nature Materials*, 2013, **12**, 518-522.
42. S. P. Ong, V. L. Chevrier, G. Hautier, A. Jain, C. Moore, S. Kim, X. Ma and G. Ceder, *Energy Environ Sci*, 2011, **4**, 3680-3688.
43. C. Xuan, *Journal of the Electrochemical Society*, 2013, **160**, A3048-A3053.

Graphical Abstract



2D amorphous iron phosphate nanosheets coated carbon exhibits high rate capability and ultra-long cycle life for sodium ion batteries.